



A Study on the Motion of High Speed Supercavitating Projectiles

H. Forouzani¹, B. Saranjam^{1†} and R. Kamali²

¹ *Department of Naval Engineering, Malek Ashtar University of Technology, Shiraz 71855465, Iran.*

² *School of Mechanical Engineering, Shiraz University, Shiraz, Iran*

† *Corresponding Author Email: b_saranjam@yahoo.com*

(Received January 20, 2018; accepted May 13, 2018)

ABSTRACT

In the last two decades much research works have been performed in order to model the dynamics of high-speed supercavitating projectiles. In the present study, the high speed supercavitating projectiles have been investigated analytically. In this context, the equations of motion were developed for the projectile inside the supercavity. To achieve this purpose, the projectile is described by its mass, geometry and moment of inertia relative to a body-fixed coordinates system. Two experimental based models were used for simulation of supercavity dynamics and the planing force. Furthermore, a detailed parametric study was performed to investigate effect of three main parameters including the mass, cavitator diameter and length of projectile, on the flight performance of a high speed supercavitating projectile. Results obtained in this parametric study can provide some physical insights into high-speed supercavitating projectile design.

Keywords: Supercavitation; Supercavitating projectile; Cavity dynamics; Planing force.

NOMENCLATURE

A_{cav}	cavitator area	R	cylinder radius
C_D	cavitator drag coefficient	R_o	cavitator radius
d_{cav}	cavitator diameter	R_c	cavity radius
F_i	i component of the external force	s	position vector
F_p	planing force	u	velocity in the x direction
h'	immersion depth	v	velocity in the y direction
I	moment inertia	V	velocity vector
l	projectile length	w	z component of the velocity
L_c	supercavity length	X_i	inertial coordinate component
m	projectile mass	x	body coordinate component
M_i	i component of the moment vector	θ	immersion angle
P	pressure	ρ	water density
p	angular velocity in the x direction	σ	Cavitation number
q	angular velocity in the y direction	ω	angular velocity
r	angular velocity in the z direction	Ω	skew-symmetric form of angular velocity

1. INTRODUCTION

When a high speed object moves in water, the water pressure will be reduced to vapor pressure in localized regions and cavities containing water vapor will form. If a whole object is entirely surrounded by a huge cavity, this phenomenon is called supercavitation. Supercavitation phenomenon has important applications in drag reduction. This effect is used to reduce skin friction drag of the High-Speed Supercavitating Projectiles (HSSPs). HSSPs are high speed under-

water projectiles which are completely surrounded by a supercavity (Nguyen *et al.* 2011). By the formation of cavity, only small portions of projectile in the nose and sometimes at the tail are in contact with water which results in significant reduction of skin friction drag. Existing initial launch disturbances and the gravity effect often lead to rotation of projectile inside the cavity and impact with the cavity surface, the so called "tail slap". The planing forces and moments are significant features and can affect the projectile motion.

Although the wetted area in the tail region is very small, the restoring forces and moments are considerable and can affect projectile dynamics (Seon and Nakwan 2015). The schematic model of the projectile with some variables describing the motion has been depicted in Fig. 1. The projectile geometry shown in the figure is notional.

To date, considerable efforts have been made to model HSSPs dynamics. The main differences between these models are the geometry and dynamics of the cavity, the planing forces and the cavitator forces. Kulkarni and Pratap (2000) used a simple model based on the concept of flow planes to determine the forces acting on the projectile during impact. They modeled the planing force in the tail region as an impact with a rigid barrier with variable coefficient of restitution and proposed a functional form of the coefficient of restitution. Kirichner *et al.* (2002) also modeled the planing force based on the angle of attack and the immersion depth of the aft in the cavity. In a similar work Fine and Kinnas (1993) studied the planing force and moment for a cylinder as functions of the angle of attack, immersion depth, the curvature of the fluid surface in the planing region and the cavitation number.

In this respect, Dzielski and Kurdila (2003) established a planing force model based on Logvinovich's work (1980) and as a function of immersion angle and depth. This model is linear when the projectile is not in contact with the cavity wall or when the planing force does not exist. Kirischner *et al.* (2003) also modeled the planing force as a force derived from the combination of a nonlinear and non-smooth spring and a damper.

As mentioned earlier, another difference between the supercavitating projectile models is the geometry and dynamics of the cavity. Many efforts devoted to studying the cavity behavior are widely based on two main methods: the computational fluid dynamics (CFD) and the boundary element method (BEM) (Mirzaei *et al.* 2015). CFD method is more accurate than BEM, but it requires a higher computational cost (Yu *et al.* 2012; Pan *et al.* 2010).

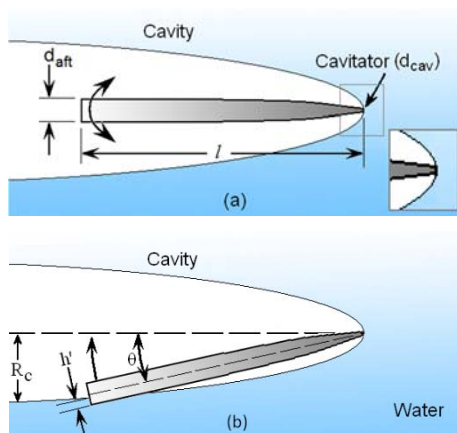


Fig. 1. Supercavitating projectile dynamics (a) only nose is in contact with water (b) both nose and tail are in contact with water

Another advantage of CFD method is their ability to

simulate a wide range of cavitation numbers and especially the cases of extremely small cavitation numbers (Chen and Lu 2008). In contrast, the improved BEM can model the cavity behavior with sufficient accuracy in relatively lower computational time (Kirschner *et al.* 1995; Nouri and Eslamdoost 2009).

Despite different models for cavity dynamics and planing force, Mirzaei *et al.* (2015) studied a new method for modeling HSSP. They considered three models for planing force and three models for cavity shape. In doing so, they selected the most appropriate model for the cavity shape by considering two experimental test cases. The experiments were done at the MIT Rifle Range facility on 0.22 caliber projectiles using high-speed digital imaging (Truscott 2009). They also studied two conventional models and one empirical model for planing force with the selected cavity shape model to investigate the most suitable model for the planing force. Some parameters such as longitudinal motion (x) and speed in x -direction, depth and speed in depth direction, pitch angle, radius of cavity and cavity centerline angle, were directly obtained from the experimental test data (as the videos of projectile motion) and they were compared with the models. Data derived from the experimental pitch angle for the planing force had enough accuracy because the only moment applied on the projectile was due to the planing force. Finally the most suitable models for the planing force and the cavity shape were chosen.

Having searched the published literature, almost no parametric study on HSSP has been identified. Hence, in order to fulfill the objective of this study, a detailed parametric study was performed on HSSP in which the effect of three main parameters including mass, cavitator diameter and length on dynamics of a supercavitating projectile were investigated.

Given the best selected models for planing force and the cavity shape based on the work of Mirzaei *et al.* (2015), this paper aims to simulate the dynamics of HSSP. Therefore, in the next section, a detailed description of these models is provided.

2. MODELING OF THE SUPERCAVITATING PROJECTILE

2.1 Equations of Motion

In full DoF model, the forces exerted on the projectile are the drag force in the nose, the gravitational force (weight) and the planing force in the aft. The moments applied on the projectile about the cavitator are due to the planing and gravitational forces. A schematic representation of the definition of the coordinate systems is depicted in Fig. 2. As shown, two coordinate systems, namely an earth-fixed or inertial coordinate system (inertial frame) with the origin at sea level and a body-fixed coordinate system (body frame) with the origin at projectile nose are considered. The projectile nose is chosen as the origin of the body frame because

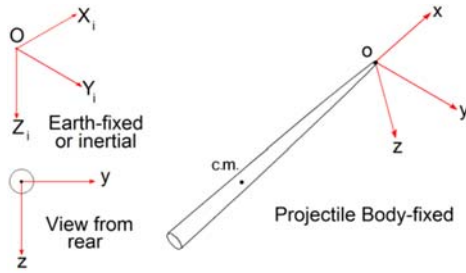


Fig. 2. Inertial and body coordinate systems

the cavitator does not produce any moment about that point and the pitch rate has no effect on the cavitator force, which results in simpler equations.

The Newton’s second law is the most important tool for modeling projectile flight dynamics. It governs the motions of the center of mass (c.m.) of the projectile subjected to external forces. This law is applied in inertial frame, thus to drive the equations of motion for the projectile With Respect To (WRT) arbitrary reference point in body frame such as cavitator, the Grubin’s transformation of Newton’s law was used (Zipfel 2007).

The equations of motion for a supercavitating projectile have been provided and are given in Eqs. (1) and (2). Equation (1) represents the Grubin’s transformation of the linear momentum equations and describes the translational motion of projectile and Eq. (2) represents the Grubin’s transformation of the angular momentum equations which describes the rotational motion about the body frame.

$$\left[\frac{d}{dt}V_o^I\right]^B = \frac{[F]^B}{m} - [\Omega^{BI}]^B [\Omega^{BI}]^B [s_{ocm}]^B - \left[\frac{d}{dt}\Omega^{BI}\right]^B [s_{ocm}]^B - [\Omega^{BI}]^B [V_o^I]^B \quad (1)$$

$$\left[\frac{d}{dt}\omega^{BI}\right]^B = \left([I_o^B]^B\right)^{-1} \left([M_o]^B - m [s_{ocm}]^B \left(\left[\frac{d}{dt}V_o^I\right]^B + [\Omega^{BI}]^B [V_o^I]^B \right) \right) \quad (2)$$

Where m is the mass, $[s_{ocm}]^B$ is the position of point o WRT point $c.m.$ in the body frame, $[F]^B$ is the external force in body frame, $[M_o]^B$ is the moment about point o in the body frame, $[V_o^I]^B$ is the velocity of point o WRT inertial frame expressed in body frame, $[\omega^{BI}]^B$ is the angular velocity of body frame WRT inertial frame expressed in body frame, $[\Omega^{BI}]^B$ is skew-symmetric form of angular velocity of body frame WRT inertial frame expressed in body frame and $[I_o^B]^B$ is the moment of inertia of body about point o in body frame. As shown in Fig. 3 for a supercavitating projectile, the motion parameters are:

$$[s_{ocm}]^B = \begin{bmatrix} x_{ocm} \\ y_{ocm} \\ z_{ocm} \end{bmatrix} = \begin{bmatrix} L \\ 0 \\ 0 \end{bmatrix} \quad (3)$$

$$[V_o^I]^B = \begin{bmatrix} u \\ v \\ w \end{bmatrix} = \begin{bmatrix} U \\ 0 \\ W \end{bmatrix} \quad (4)$$

$$\left[\frac{d}{dt}V_o^I\right]^B = \begin{bmatrix} \dot{u} \\ \dot{v} \\ \dot{w} \end{bmatrix} = \begin{bmatrix} \dot{U} \\ 0 \\ \dot{W} \end{bmatrix} \quad (5)$$

$$[\omega^{BI}]^B = \begin{bmatrix} p \\ q \\ r \end{bmatrix} = \begin{bmatrix} 0 \\ Q \\ 0 \end{bmatrix} \quad (6)$$

$$\left[\frac{d}{dt}\omega^{BI}\right]^B = \begin{bmatrix} \dot{p} \\ \dot{q} \\ \dot{r} \end{bmatrix} = \begin{bmatrix} 0 \\ \dot{Q} \\ 0 \end{bmatrix} \quad (7)$$

$$[\Omega^{BI}]^B = \begin{bmatrix} 0 & -r & q \\ r & 0 & -p \\ -q & p & 0 \end{bmatrix} = \begin{bmatrix} 0 & 0 & Q \\ 0 & 0 & 0 \\ -Q & 0 & 0 \end{bmatrix} \quad (8)$$

$$\left[\frac{d}{dt}\Omega^{BI}\right]^B = \begin{bmatrix} 0 & -\dot{r} & \dot{q} \\ \dot{r} & 0 & -\dot{p} \\ -\dot{q} & \dot{p} & 0 \end{bmatrix} = \begin{bmatrix} 0 & 0 & \dot{Q} \\ 0 & 0 & 0 \\ -\dot{Q} & 0 & 0 \end{bmatrix} \quad (9)$$

$$[I_o^B]^B = \begin{bmatrix} I_{xx} & 0 & 0 \\ 0 & I_{yy} & 0 \\ 0 & 0 & I_{zz} \end{bmatrix} \quad (10)$$

$$[F]^B = \begin{bmatrix} F_x \\ F_y \\ F_z \end{bmatrix} \quad (11)$$

$$[M_o]^B = \begin{bmatrix} M_x \\ M_y \\ M_z \end{bmatrix} \quad (12)$$

Applying these definitions into Eqs. (1) and (2), the equations of motion for the projectile will be obtained as follows:

$$\begin{cases} \dot{U} = \frac{F_x}{m} + Q^2 L - QU \\ \dot{W} = \frac{F_z}{m} + \dot{Q} L + QU \\ I_{yy} \dot{Q} = M_y + mL(\dot{W} - QU) \end{cases} \quad (13)$$

The dynamic equations can be rewritten in the following compact form:

$$\begin{bmatrix} m & 0 & 0 \\ 0 & m & -mL \\ 0 & -mL & I_{yy} \end{bmatrix} \begin{bmatrix} \dot{U} \\ \dot{W} \\ \dot{Q} \end{bmatrix} = Q \begin{bmatrix} 0 & -m & mL \\ m & 0 & 0 \\ -mL & 0 & 0 \end{bmatrix} \begin{bmatrix} U \\ W \\ Q \end{bmatrix} + \begin{bmatrix} F_x \\ F_z \\ M_y \end{bmatrix} \quad (14)$$

In Eq. (14), the body frame force in the x -direction, F_x , consists of both cavitator force and x -component of the body frame gravity force (Eq. (15)). The body frame force in the z -direction, F_z , consists of z -component of the body frame gravity force and the planing force (Eq. (16)). A schematic model of these forces has been represented in Fig. 4. As mentioned, the body-frame pitching moment consists of moments caused by the gravitational force and the planing force. These forces and moments will be described in the following sections.

$$F_x = F_{cav} + F_{xg} \quad (15)$$

$$F_z = F_p + F_{zg} \quad (16)$$

$$M_y = M_p + M_g \quad (17)$$

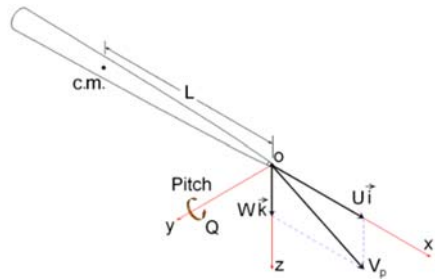


Fig. 3. Motion parameters of a supercavitating projectile

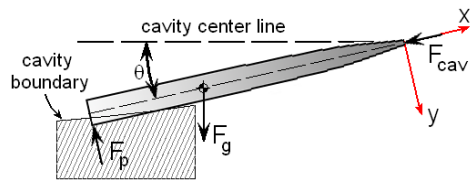


Fig. 4. Forces acting on a supercavitating projectile

In the case that the supercavitating projectile is moving in one phase media such as air, its motion dynamics should be calculated similar to airborne bullet. Unlike airborne bullet, supercavitating projectiles have no spin rotation and its stability is secured by tail slap phenomena. Due to lack of supercavity, there is no tail slap, and its stability depend on the center of gravity and center of pressure locations. In the stable condition, the center of gravity is ahead of the center of pressure. The experimental data show that the axisymmetric projectile center of pressure (similar to HSSP) is ahead of the center of gravity (Nielsen, J. N. 1960). Hence, these projectiles are unstable. In practice, it is necessary for airborne supercavitating projectile to install fins at the end of projectile in order to eliminate instability.

2.2 Cavitator Force Modeling

The cavitation number is used to characterize the potential of the flow to cavitate and is defined as a function of the local absolute pressure P_∞ , the vapor pressure of liquid P_v , the fluid density ρ and the projectile velocity magnitude V .

$$\sigma = \frac{P_\infty - P_v}{0.5\rho V^2} \quad (18)$$

When the supercavitating projectile is fully contained in the cavity, the only active hydrodynamic force is on the cavitator. The cavitator force is a function of cavitation number, the cavitator angle of attack to the flow which is equal to zero for a HSSP, and the cavitator drag coefficient (Kirschner *et al.* 2003). The forces acting on a disk-type cavitator of a HSSP in a steady flow are well understood as it may be assumed that the force vector is normal to the wetted surface and acts through the center of the disk. This force for a disk-type cavitator is given by Eq. (19) (Seon and Nakwan 2015):

$$F_{cav} = \frac{1}{2} \rho V^2 A_{cav} C_D \quad (19)$$

Where A_{cav} is the cavitator surface area, V is the magnitude of the projectile's velocity at the cavitator, C_D is the cavitator drag coefficient and ρ is the fluid (water) density. The cavitator drag coefficient for a HSSP has been found experimentally as

$$C_D = C_{D_0} (1 + \sigma) \quad (20)$$

Where C_{D_0} is the drag coefficient at zero angle of attack and cavitation number, and is taken equal to 0.82 based on experimental data (Dzielski 2003).

2.3 Planing Force Modeling

In the case of a supercavitating projectile, unlike a fully wetted projectile the stability does not depend solely on the hydrodynamic coefficients, but rather on the moments exerted on the nose and the aft of the projectile. As mentioned earlier, a HSSP which is travelling on a direct path often starts to rotate towards the up and down sides of the cavity and hits the cavity wall resulting in formation of the planing force. Thus, the planing force is a function of immersion depth of the projectile in the cavity which in turn is proportional to the cavity shape and size and the projectile position, too (Wosnik and Arndt 2009). The planing force has been shown in Fig. 4.

Mirzaei *et al.* (2015) considered three different models for planing force and moment based on the works of Logvinovich (Mao 2010), Hassan (Geol 2005, Cameron 2009) and Yen *et al.* (2011). However, Logvinovich and Hassan models are analytical models based on the fluid dynamics; and while the planing forces in these two models are equal, the planing moments are different. These differences are due to viscous effect considerations suggested by Hassan's model. In this model the effects of skin friction are taken into account. In contrast, the developed model by Yen *et al.* (2011) is an empirical model based on experiments on a cylinder conducted at the Davidson Laboratory high-speed towing tank facility at Stevens Institute of Technology. Mirzaei *et al.* (2015) showed that this model in conjunction with the developed cavity model by Zhang *et al.* (2011) and Guo *et al.* (2012) has a good agreement with experimental results. Therefore in the present study, these models are used for simulation of planing force and cavity shape, respectively. The empirical formulas for planing force based on the work of Yen *et al.* (2011) are as follows:

$$F_p(\alpha) = F_{dynamic} + F_{buoyancy} \quad (21)$$

Where:

$$F_{dynamic} = 0.45\rho V^2 R^2 \theta^{0.9} \left(\frac{2hr'}{R}\right)^{0.64} \quad (22)$$

$$F_{buoyancy} = 8.95\rho g \frac{hr'^{2.9}}{\theta^{1.36}} \quad (23)$$

In the above equations, θ is the immersion angle in radians and h' is the immersion depth (see Fig. 1), which are calculated from following equations:

$$\theta = \begin{cases} \frac{w}{V} - \frac{\dot{R}_c}{V} & w > 0 \\ \frac{w}{V} + \frac{\dot{R}_c}{V} & w \leq 0 \end{cases} \quad (24)$$

$$h' = \begin{cases} 0 & |w| \leq \frac{V(R_c - R)}{l} \\ 1 \left| \frac{w}{V} \right| - (R_c - R) & |w| > \frac{V(R_c - R)}{l} \end{cases} \quad (25)$$

Where w reflects the velocity in z -direction, R_c and \dot{R}_c are the cavity radius and the contraction rate of cavity radius in the aft region. The planing moment is given as:

$$M_p = F_p(\alpha) \times l \quad (26)$$

Where l is the length of projectile.

2.4 Cavity Dynamic Modeling

The shape of the cavity is the main feature in the simulation of the planing force of a supercavitating projectile. *Mirzaei et al. (2015)* presented three cavity models based on the works of *Logvinovich (1980)*, *Savchenko (Vlasenko 2003)* and *Zhang et al. (2011)*. *Logvinovich's* model assumes that the expansion of each section of cavity is independent of the neighbor sections without considering the viscous effects (*Logvinovich independence principle*). *Savchenko* has developed an empirical formula to calculate the shape of cavity in the supercavitation regime. *Zhang et al. (2011)* have introduced a cavity model based on the experimental considerations and the solution to the Rayleigh-Besant problem, too. They showed that the obtained results were truly in accordance with the experimental results.

Mirzaei et al. (2015) regarded the three mentioned models for the cavity shape and compared the simulation results with experimental results obtained from the work of *Truscott (2009)* on 0.22 caliber projectiles at the MIT Rifle Range facility. They indicated that the introduced cavity model by *Zhang et al.* has very good compatibility with the experimental results. In this paper, the developed model by *Zhang et al. (2011)* was taken into account for the simulation of cavity shape. In this model, the cavity radius is defined as:

$$R_c = \sqrt{R_o^2 + 2R_o \sqrt{\frac{K}{2N}}(x - x_o) - \frac{\sigma}{2N}(x - x_o)^2} \quad (27)$$

Where, R_o is the cavitator radius, $x_o = 0$, $K = 0.835$ and is the drag coefficient, N is a constant and equal to 1.4, σ is the cavitation number and x is the distance from the cavitator. For calculation of the cavity radius in the tail region, x is equal to l (length of projectile). This is further illustrated by an example in which the cavity shape for a projectile with $R_o = 1$ mm is computed using this model and is shown in Fig. 5.

As can be observed in this figure, the effect of cavitation number on the cavity shape increases with increasing the distance from the nose, therefore, this effect is high in the tail contact region.

In this study, the *Zhang* ellipsoidal cavity model was utilized for supercavity shape prediction. In the studied range of HSSPs motion, the main

characteristic feature of such supercavities are their very large aspect ratio, $\lambda = L_c/D_c \leq 400$. For example, the length of a supercavity (L_c) was formed by a HSSP with the disk cavitator (radius $R_o = 0.75$ mm) at velocity $V = 1500$ m/s, is equal to 33.1 m, whereas the HSSP length is only 0.15-0.2 m and the closure is very far from HSSP. Moreover, In the case of slender cavities, point closure is used where back closure action is modeled by source of pressure which is follow automatically on the base of Slender Body Theory expansions. For HSSP flow modeling we have not back response of flow to its forward part and back closure is not required.

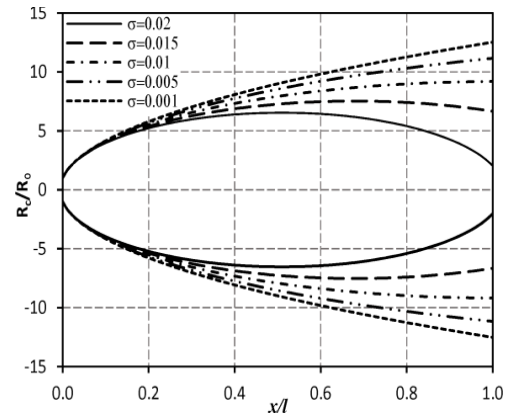


Fig. 5. Effect of cavitation number on the shape

3. RESULTS AND DISCUSSION

In order to perform a detailed parametric study on the HSSPs, as the first step, the simulation results have been compared with the experimental data which has been presented by *Truscott et al. (2009)*. They experimentally investigated the flight of 0.22 caliber modified projectiles at the MIT Rifle Range facility. The projectile was shot into a water tank by a pneumatic gun and its behavior such as location and speed, were recorded by a high speed digital camera. The experimental test case characteristics have been presented in Table 1.

The comparison of the experimental measurements and simulation predictions of the 0.22 caliber modified projectile range and velocity in terms of time are shown in Figs. 6 and 7. It should be noted that in these experiments, data are measured up to 4.5 millisecond times. Therefore the simulation calculations are performed up to this time, too. As it has been shown in these figures, it can be seen that the present simulation results agree fairly well with experimental data.

As aforementioned, the review of the related existing literature indicated that there was almost no parametric study on HSSP. Hence, in this section, the effects of three main parameters i.e. the mass, cavitator diameter and the length, on dynamics of a supercavitating projectile have been investigated. The geometry and dimensions of the projectile have been demonstrated in Fig. 8. As it is indicated, the projectile shape is similar to a truncated cone.

Table 1 Experimental test case characteristics

Description	Value and units
Projectile mass	2.66 gr
Projectile radius	0.28 cm
Projectile length	4 cm
Cavitator radius	0.28 cm
Gravitational acceleration	9.81 m/s ²
Initial axial velocity	225 m/s
Final time	5 ms
Initial pitch angle	11°

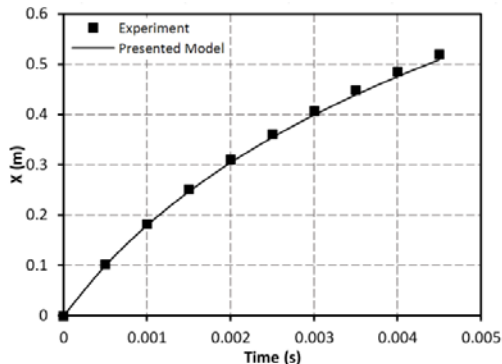


Fig. 6. Comparison of the experimental data and simulation predictions of the 0.22 caliber modified projectile range versus time

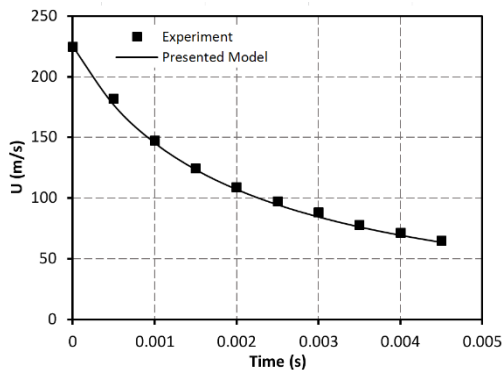


Fig. 7. Comparison of the experimental data and simulation predictions of the 0.22 caliber modified projectile velocity versus time

3.1 Mass of the Projectile

In order to investigate the effect of the mass of projectile, four projectiles of the same dimensions but different materials, Aluminum, Titanium, Steel and Tungsten as the cases 1 to 4, were applied. The geometry of projectiles was similar to a frustum of cone with base (aft) diameter of 10 mm, nose (cavitator) diameter of 1.5 mm and length of 150 mm. According to the dimensions of the projectiles and density of each material, the mass of the four cases has been presented in Table 2. The numerical examples used in the following simulations were based on the parameter values given in Table 3.

The results have been presented in Fig. 9. It should be noted that the simulations have been carried out for final axial velocity limit of 200 m/s or final time limit of 0.5 s. The x-location or range of the four

cases versus time has been depicted in Fig. 9a. As can be seen, by keeping all other parameters as constant, the heavier the projectile is, the higher the range. The reason is that, by increasing the mass of projectiles and the same initial axial velocity for these projectiles, the kinetic energy is greater for the heavier ones. In addition, as Fig. 9c indicated, it is clear that, as the mass of projectile increases, so does the time to reach the final velocity limit. In Fig. 9c, it can be seen that the axial speed of heavier projectiles is higher in all times. However, higher axial velocity in all times, results in more drag force in all times. It is because the speed decreases accordingly via the cavitator drag force, which is the result of considering supercavity phenomenon for projectiles. Figure 9h shows that the initial drag force is similar for all the cases because of the same initial speed. But in the later times, the drag force is greater for the heavier projectile, since its speed is higher than the others.

The path trajectory for these cases has been shown in Fig. 9b. It is revealed that the deviation from straight path for heavier cases is less than the lighter ones at the beginning range of the motion. The one factor of note is that the initial depth is considered to be 1.0 m. Further examination of the graph indicates that as

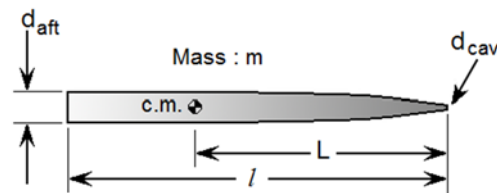


Fig. 8. Geometry and dimensions of the projectile parametric study

Table 2 PROJECTILES characteristics with different mass

Case NO.	Material	d_{aft} (mm)	d_{cav} (mm)	l (mm)	m (kg)	ρ (kg/m ³)
1	Aluminum	10	1.5	150	17	2700
2	Titanium	10	1.5	150	28	4500
3	Steel	10	1.5	150	48	7800
4	Tungsten	10	1.5	150	119	19000

Table 3 Parameters for simulation models

Parameter	Description	Value and units
g	Gravitational acceleration	9.81 m/s ²
Z_0	Initial depth	1.0 m
U_0	Initial axial velocity	1500 m/s
U_f	Final axial velocity	200 m/s
t_r	Final time	0.5 s
θ_0	Initial pitch angle	0°
Q_0	Initial angular velocity	1 rad/s
W_0	Initial vertical velocity	0 m/s

the mass increases, so does the final depth. Moreover, in various projectile weights, the differences between the depths locations occurred primarily because of the differences in planing forces (see Fig. 9g). Then, the motion trajectory of the projectiles is affected by the gravitational and planing forces.

The z-velocities versus time have been displayed in Fig. 9d. According to Fig. 9d, the changes in z-velocity are apparent at any time when the impact with cavity wall has occurred. Moreover, it can be noticed that the rate of changes in z-velocity for all the cases is higher at the beginning of the motion, which is due to higher magnitudes of planing forces. On the other hand, by increasing the mass of projectiles, both the number of projectile impacts to cavity wall and the z-velocity limits rise.

Figures 9e and 9f show the pitch angle and angular velocity of projectiles, respectively. It can be found from Fig. 9e that in planing zone, the changes in the pitch angle come to an end and the planing on the cavity wall forces the projectile to begin to pitch in the opposite side. Furthermore, it is clear from Fig. 9f that the direction of the angular velocity has changed during each planing and the magnitude of the angular velocity has remained almost constant between two planings. Figure 9f also indicates that after each impact, the magnitude of angular velocity has decreased. For example, the magnitude of angular velocity for the Tungsten projectile is about 0.78, 0.55, 0.45 and 0.3 rad/s after the first, second, third and fourth planings, respectively. These values for the Steel projectile are almost similar after its three planings. However, it is clear that the reduction in the angular velocity of lighter projectile after the first planing is less than the heavier ones. As mentioned, the reason is because of the difference between the magnitudes of planing forces for various projectiles (see Fig. 9g).

Figure 9g presents the planing force for all the cases versus time. Based on this graph, it is obvious that the number of impacts for the heavier projectiles is more than lighter ones. Moreover, it can be seen that the magnitude of planing force is greater for the heavier projectile. This result can be explained by the fact that according to Eqs. (22) and (23), the planing force is related to the immersion depth and velocity magnitude of the projectile. Moreover, while the difference between immersion depths for projectiles is negligible, the difference between the velocity magnitudes before the first planing is considerable. Accordingly, the velocity magnitude is greater for the heavier projectiles which results in the greater magnitudes of planing force for them. The planing force also is alternately positive and negative which is due to the contact of projectile with the cavity inside the surfaces.

3.2 Cavitator Diameter

In order to examine the effect of cavitator diameter on dynamics of a supercavitating projectile, four projectiles with the same geometry and material but different cavitator diameters of 1.5, 2.0, 2.5 and 3.0 mm were studied. The characteristics of the

projectiles have been presented in Table 4 and other parameters are the same as the Table 3.

The simulation results have been displayed in Fig. 10. As it is obvious, in Fig. 10a, the axial range of the projectile experiences a significant reduction by increasing the cavitator diameter which is due to the considerable increase of the drag force as expected by the increase in surface area at the nose which is in contact with water (see also Fig. 10h). According to Fig. 10h, although the initial drag force is greater for the projectiles with bigger cavitator diameter, the slope of reduction in the drag force is steeper for them, which is due to the sudden reduction in the speed of projectile.

The x-velocity of these cases versus time has been presented in Fig. 10c, too. More examinations have demonstrated that by increasing the cavitator diameter, the reduction in axial velocity will be steeper, and also the projectile will sooner reach the final velocity limit of 200 m/s.

Figure 10b presents the path trajectories for these cases. It implies that the deviation from straight path for case 3 is less than the other cases at the beginning range of the motion. Thus, by increasing the cavitator diameter, deviation from straight path in the projectiles trajectory increased. Moreover, it shows that the trend of the projectiles behavior is similar and by decreasing the cavitator diameter, the final depth location has increased.

Table 4 Projectiles characteristics with different cavitator diameter

Case No.	d_{aft} (mm)	d_{cav} (mm)	l (mm)	m (gr)
3	10	1.5	150	48
5	10	2.0	150	48
6	10	2.5	150	48
7	10	3.0	150	48

The z-velocity changes versus time are seen in Fig. 10d, too. According to this graph, changes in the z-velocity are obvious during the planing of the projectiles with the cavity wall and any increase in cavitator diameter will expand the z-velocity changes domain.

Figures 10e and 10f also demonstrate the pitch angle and angular velocity of the four cases, respectively. Interestingly, these figures show that the direction of the pitch angle and angular velocity have changed during each planing, however, the magnitude of the angular velocity has remained almost constant between two planings. From Fig. 10f, it is noticeable that for the projectile with 1.5 mm cavitator diameter, the magnitude of the angular velocity decreased from 1 rad/s to about 0.8 rad/s after the first planing. However, for the projectile with 3.0 mm cavitator diameter, the magnitude of the angular velocity increased from 1 rad/s to about 2.1 rad/s after the first planing.

Kulkarni and Pratap (2000) have suggested that the

angular velocity of the supercavitating projectile may increase, decrease or be constant during an impact with the cavity wall. They presented a criterion for the change in the angular velocity during the impact as follows:

$$\left| \frac{Q^+}{Q^-} \right| > 1 \quad \text{when} \quad \frac{LQ^-}{U-\theta} < \frac{x_{c.m.}}{L} \ln \frac{G}{2-G} \quad (28)$$

$$\left| \frac{Q^+}{Q^-} \right| \leq 1 \quad \text{when} \quad \frac{LQ^-}{U-\theta} \geq \frac{x_{c.m.}}{L} \ln \frac{G}{2-G} \quad (29)$$

Where Q^- and Q^+ are the angular velocity of the projectile before and after impact, respectively, U^- is the x-velocity before impact, θ is the angle of impact, $x_{c.g.}$ is the distance between the aft and c.m. and $G = mx_{c.m.}L / (I_y + mx_{c.g.}^2)$.

Figure 10g represents the planing force for all the cases versus time. Based on this graph, it is evident that the number of impacts for the projectiles with 1.5, 2.0, 2.5 and 3.0 mm cavitator diameter is equal to 3, 2, 1 and 1, respectively, until the projectiles have reached the final limiting speed of 200 m/s. Moreover, it can be found that the magnitude of planing force is greater for the projectile with less cavitator diameter. The planing force is again alternately positive and negative due to change in the direction of contact with the cavity wall.

This result can be justified using Eq. (25) which shows that increasing the velocity magnitude of the projectile before the impact leads to the reduction in immersion depth. Further, it can be seen in Fig. 10g that the magnitude of planing force is about 34 and 22 N for the first planing of projectiles with 1.5 and 3.0 mm cavitator diameters, respectively. In addition, it is clear from Fig. 10g that the magnitude of planing force for the projectile with smaller cavitator diameter has a moderately decreasing trend which is due to the reduction in the velocity magnitude of the projectile and the immersion depth (see Eqs. (22) and (23)).

3.3 Length of the Projectile

In order to investigate the effect of the length parameter on the dynamics of a supercavitating projectile, four projectiles of the same mass (48 gr) and cavitator diameter, but different lengths of 75, 100, 150 and 200 mm have been taken into account. The cavitator diameter was considered as 1.5 mm for all the cases. It should be noted that by changing the length of the projectile while keeping the mass as constant, the moment of inertia (about y-axes) and the location of the center of gravity WRT the aft will change, too. The characteristics of these projectiles have been provided in Table 5.

The results of simulation have been presented in Fig. 11. The x-location, x-velocity and drag of the considered projectiles have been shown in Fig. 11a, 11c and 11h, respectively. As is illustrated, the results for all the projectiles coincided completely. The reason is that the mass and the initial velocity are the same for all the projectiles and the only difference between them was their length. As already mentioned, changing the length of the

projectile will alter the moment of inertia about the y-axes and the location of c.m.. Therefore, the consequence of any changes in the length (without changing any other parameter), will appear primarily in changes in the planing force and planing moment. According to this finding, it is obvious that the planing force and planing moment have a little efficacy on the x-location and x-velocity of the projectiles, which lead to agreement in the results for all the cases.

The path trajectories for all the cases have been represented in Fig. 11b. According to this graph, the changes in the depth locations and path trajectories coincide for almost all the cases at the beginning of the motion. But depth locations are deeper for longer projectile in the end of the motion. To better elucidate, the planing of projectile with the cavity wall is a mechanism for returning the projectile to the direct path motion.

The z-velocity has been depicted in Fig. 11d. According to this figure, any changes in the direction of z-velocity due to planing force are visible. As discussed earlier, longer projectiles have less number of planings which results in higher deviation of projectile from the straight path. Increasing the length of projectiles while keeping the masses as constant, leads to increasing the moment of inertia (I_{yy}) of the projectiles and hence, the longer projectiles have more stability in the motion. It can be seen in Fig. 11g that the number of planings has decreased for longer projectiles.

Figure 11g also indicates that the magnitude of planing force for the first impact is increased by increasing the projectile length. As already pointed out, the planing force is a function of immersion depth and velocity magnitude according to Eqs. (22) and (23). Although the magnitudes of velocity are almost equal for all the cases before the first impact, the magnitude of immersion depth is greater for the longer projectiles. This finding results in greater magnitudes of planing force for longer projectiles.

Table 5 Projectiles characteristics with different length

Case No.	d_{aft} (mm)	d_{cav} (mm)	L (mm)	m (gr)
8	10.0	1.5	75	48
9	10.0	1.5	100	48
3	10.0	1.5	150	48
10	10.0	1.5	200	48

4. CONCLUSIONS

In the present study, the equations of motion have been developed for the projectile motion inside the cavity. Two experimental based models have been used for simulation of the cavity shape and the planing force. Furthermore, a parametric study has been performed to investigate the effect of three main parameters which are the mass, cavitator diameter and the length, on flight performance of HSSP. The main concluding remarks drawn from the current work are provided as follows:

1. Increasing the mass of a HSSP (while keeping all the other parameters as constant), leads to higher axial ranges of projectile due to higher initial kinetic energy.
2. The deviation from straight path for heavier projectiles is less than lighter ones at the beginning
3. The range of the projectile is significantly reduced by increasing the cavitator diameter.
4. By increasing the cavitator diameter, deviation from straight path in projectiles trajectory is increased.

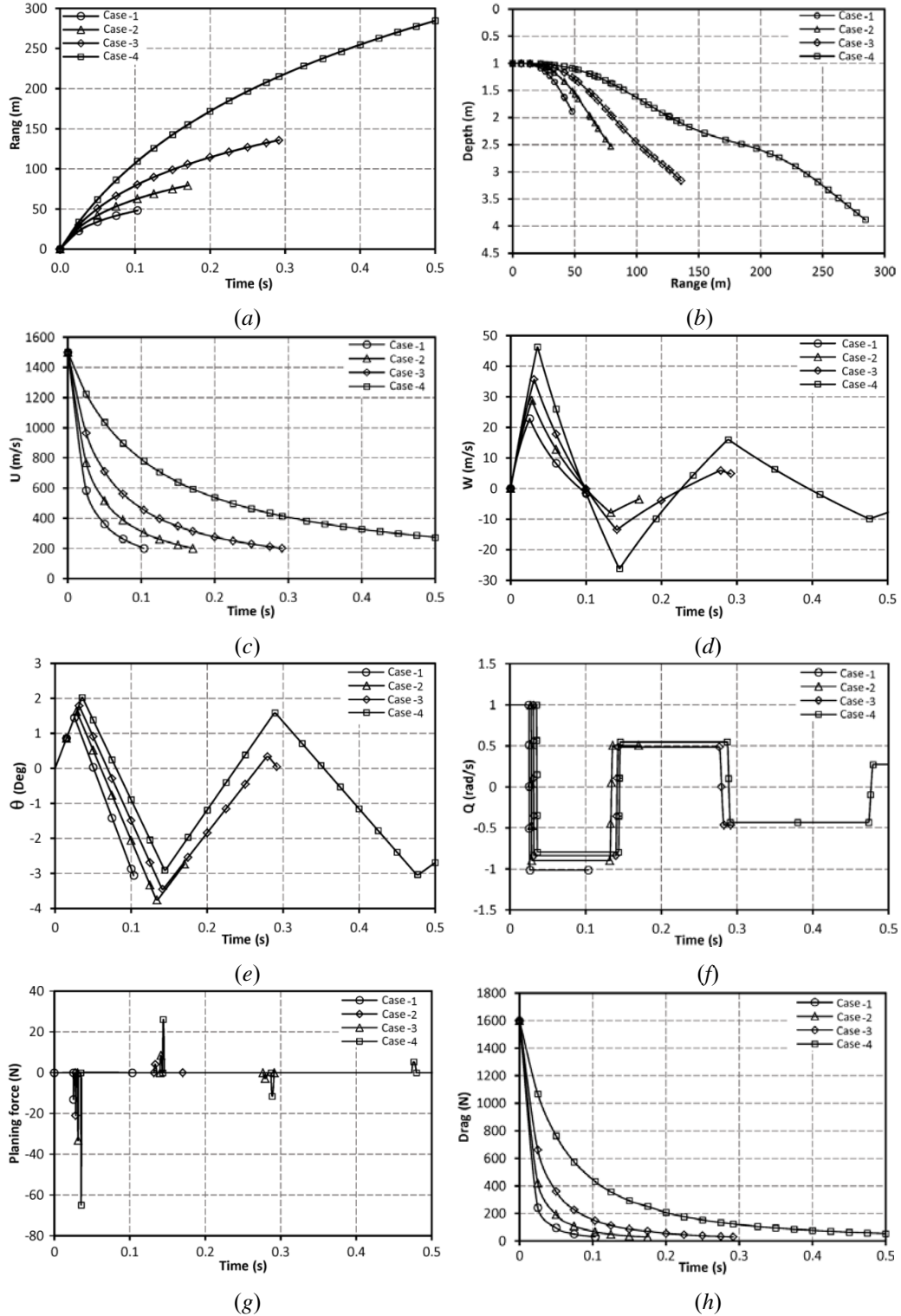


Fig. 9. Simulation results of the effect of mass variations

(a) range (m), (b) projectiles trajectories, (c) velocity in x-direction (m/s), (d) velocity in z-direction (m/s), (e) angular velocity (rad/s), (f) pitch angle ($^{\circ}$), (g) planing force (N), (h) drag force (N)

5. The HSSP length variations do not affect the range of the projectile and deviation from straight path in the operational range.

Increasing the length of a HSSP leads to reduction of the number of planings of the projectile with the cavity wall and consequently increases the stability

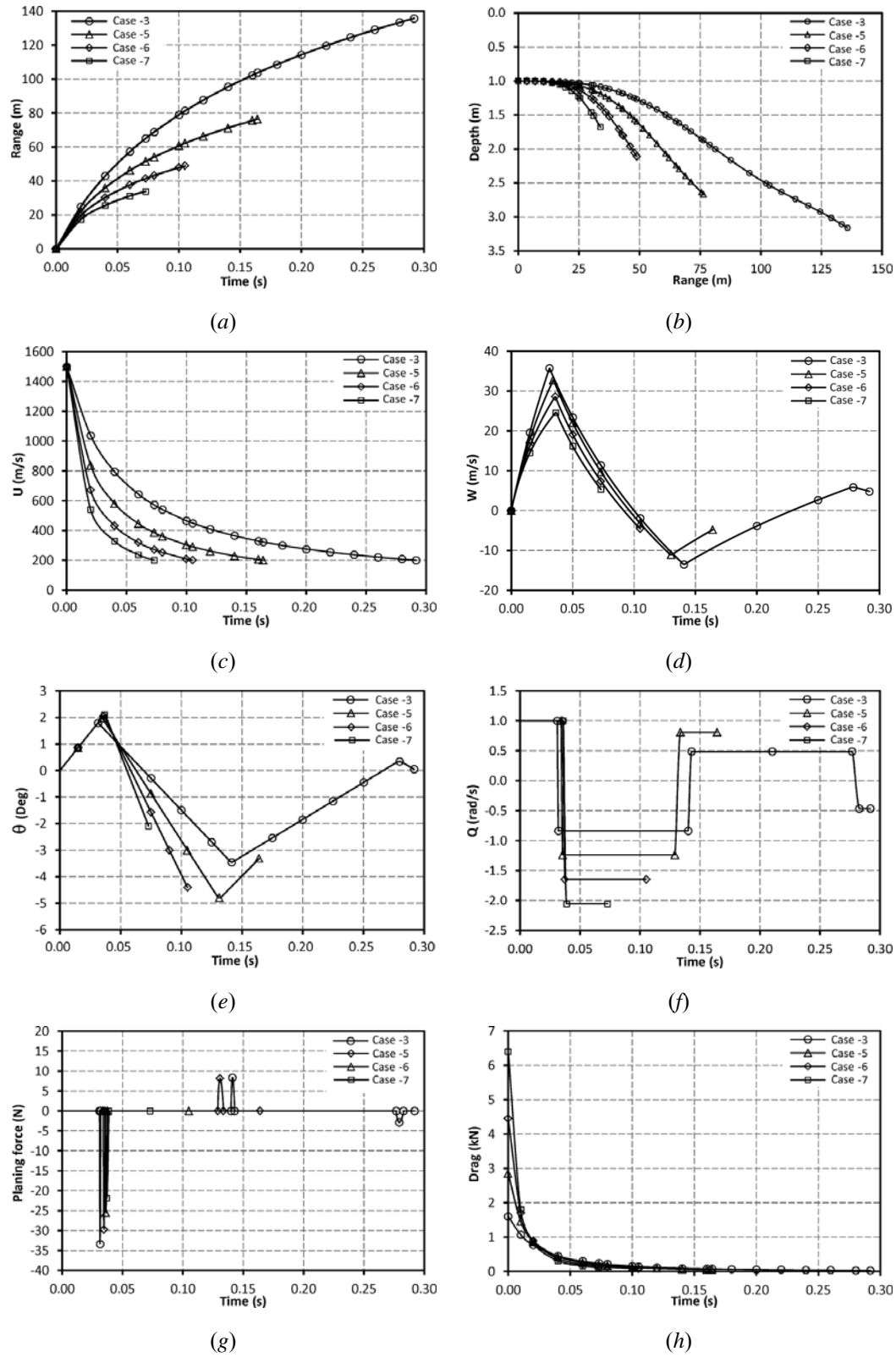


Fig. 10. Simulation results of the effect of cavitator diameter variations
 (a) range (m), (b) projectiles trajectories, (c) velocity in x-direction (m/s), (d) velocity in z-direction (m/s),
 (e) angular velocity (rad/s), (f) pitch angle (°), (g) planing force (N), (h) drag force (N)

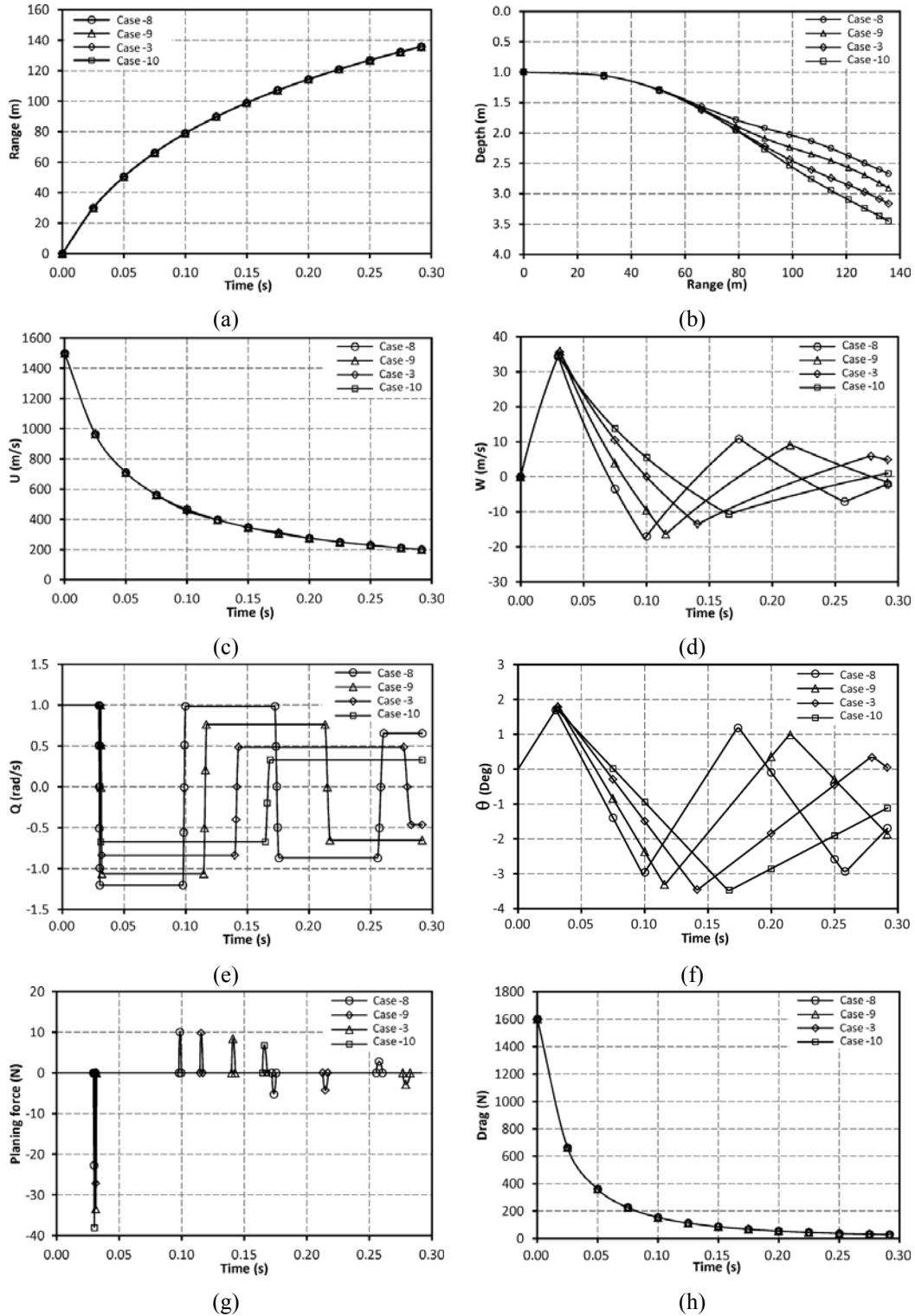


Fig. 11. Simulation results of the effect of length variation
 (a) range (m), (b) projectiles trajectories, (c) velocity in x-direction (m/s), (d) velocity in z-direction (m/s),
 (e) angular velocity (rad/s), (f) pitch angle ($^{\circ}$), (g) planing force (N), (h) drag force (N),

6. of the projectile. However, longer projectiles have higher deviations from the straight path due to less number of planings.

In practice, there are many parameters that affect the dynamics of a HSSP such as projectile impact with water free surface, behavior of the projectile

material on impact and its flexibility, local properties of water and underwater currents, etc. Last but not least, to carry out a comprehensive study on a HSSP, considering all of the variable parameters is a necessity, but is not practically possible.

5. REFERENCES

- Cameron, P. J. K. (2009). *An acoustic countermeasure to supercavitating torpedoes*. Ph.D. thesis, Atlanta, Georgia, USA: Georgia Institute of Technology.
- Chen, Y. and C. Lu (2008). A homogenous-equilibrium-model based numerical code for cavitation flows and evaluation by computation cases. *Journal of Hydrodynamics* 20(2), 186-194.
- Dzielski, J. and A. Kurdila (2003). A benchmark control problem for supercavitating vehicles and an initial investigation of solutions. *Journal of Vibration and Control* 9(7), 791-804.
- Fine, N. and S. Kinnas (1993). A boundary element method for the analysis of the flow around 3-D cavitating hydrofoils. *Journal of Ship Research* 37, 213-224.
- Goel, A. (2005). *Robust control of supercavitating vehicles in the presence of dynamic and uncertain cavity*. Ph.D. thesis, Gainesville, Florida, USA: University of Florida.
- Guo, Z., W. Zhang and C. Wang (2012). Experimental and theoretical study on the high-speed horizontal water entry behaviours of cylindrical projectiles. *Journal of Hydrodynamics* 24(2), 217-225.
- Kirschner, I. N., B. J. Rosenthal and Uhlman J. S. (2003). Simplified dynamical systems analysis of supercavitating high-speed bodies. *Proceedings of the fifth international symposium on Cavitation*, Osaka, Japan.
- Kirschner, I. N., D. C. Kring, A. W. Stokes, N. E. Fine and J. S. Uhlman (2002). Control strategies for supercavitating vehicles. *Journal of Vibration and Control* 8(2), 219-242.
- Kirschner, I.N., J. S. Uhlman, A. N. Varghese and I. M. Kuria (1995). Supercavitating projectiles in axisymmetric subsonic liquid flows. *ASME Publ Fed* 210, 75-94.
- Kulkarni, S. and R. Pratap (2000). Studies on the dynamics of a supercavitating projectile. *Journal of Applied Mathematical Modeling* 24, 113-129.
- Logvinovich, G. V. (1980). Some problems in planing surfaces. *Trudy TsAGI* 2052, 3-12.
- Mao, X. (2010). *Nonlinear robust control design for a high-speed supercavitating vehicle*. Ph.D. thesis, State College, Pennsylvania, USA: Pennsylvania State University.
- Mirzaei, M., M. Alishahi and M. Eghtesad (2015). High-speed underwater projectiles modeling: a new empirical approach. *Journal of Brazilian Society of Mechanical Sciences and Engineering* 37(2), 613-626.
- Nguyen, V. and B. Balachandran (2011). B. Supercavitating vehicles with noncylindrical, nonsymmetric cavities: dynamics and instabilities. *Journal of Computational Nonlinear Dynamics* 6, 1-11.
- Nielsen, J. N. (1960). *Missile aerodynamics*. McGRAW-HILL series in missile and space technology. New York. USA.
- Nouri, N. and A. Eslamdoost (2009). An iterative scheme for axisymmetric supercavitating flow. *Proceedings of the Institution of Mechanical Engineers, Part C: Journal of Mechanical Engineering Science* 223, 1869-1876.
- Pan, Z., C. Lu, Y. Chen and S. Hu (2010). Numerical study of periodically forced-pitching of a supercavitating vehicle. *Journal of Hydrodynamics* 22(5), 899-904.
- Seon-Hon, K. and K. Nakwan (2015). Hydrodynamics and modeling of a ventilated supercavitating body in transition phase. *Journal of Hydrodynamics* 27(5), 763-772.
- Truscott, T. T. (2009). *Cavity dynamics of water entry for spheres and ballistic projectiles*. Ph.D. thesis, Cambridge, Massachusetts, USA: Massachusetts Institute of Technology.
- Vlasenko, Y. D. (2003). Experimental investigation of supercavitation flow regimes at subsonic and transonic speeds. *Fifth International Symposium on Cavitation*. Osaka, Japan.
- Wosnik, M. and R. Arndt (2009). Control experiments with a semi axisymmetric supercavity and a supercavity-piercing fin. *Proceedings of the 7th international symposium on cavitation*. Ann Arbor, Michigan, USA.
- Yen, T., M. Morabito, L. Imas *et al.* (2011). Investigation of cylinder planing on a flat free surface. *11th international conference on fast sea transportation FAST 2011*, Honolulu, Hawaii, USA
- Yu, K., G. Zhang, J. Zhou, W. Zou and Z. Li (2012). Numerical study of the pitching motions of supercavitating vehicles. *Journal of Hydrodynamics* 24(6), 951-958.
- Zhang, W., Z. Guo, X. Xiao and C. Wang (2011). Experimental investigations on behaviors of projectile high-speed water entry. *Journal of Explosion and Shock Waves* 6, 005.
- Zipfel, P. H. (2007). *Modeling and simulation of aerospace vehicle dynamics*. AIAA, second edition, USA.